JOURNAL OF PROPULSION AND POWER
Vol. 24, No. 2, March–April 2008

Breakup of Aerated Liquid Jets in Subsonic Crossflow

B. Miller* and K. A. Sallam†
Oklahoma State University, Stillwater, Oklahoma 74078
M. Bingabr‡
University of Central Oklahoma, Edmond, Oklahoma 73034
K.-C. Lin§
Taitech Inc., Beavercreek, Ohio 45433
and
C. Carter¶
U.S. Air Force Research Laboratory, Wright–Patterson Air Force Base, Ohio 45433

DOI: 10.2514/1.30390

An experimental investigation of the breakup of an aerated-liquid jet in subsonic crossflow is described. The present test conditions were similar to those encountered in fuel injection in ramjet engines. Previous studies of spray structures of aerated-liquid jet in crossflow have been limited to the dilute spray area (downstream distance of greater than 100 jet diameters) using phase Doppler interferometry and along the liquid surface using wet holographic plates. The objective of the present study was to extend these earlier measurements to investigate the dense-spray near-injector region immediately downstream of the injector (0–50 jet diameters), in which secondary breakup may occur to bridge the gap between drop-size distributions along the jet surface and those obtained using phase Doppler interferometry in the far field of the injector. Three-dimensional microscopic digital holography was used to record and measure droplets sizes and locations within the three-dimensional volume of the spray. Earlier results of the primary breakup of aerated-liquid jets in crossflow show that the gas jet along the axis of the annular flow leaving the injector passage forces the annular liquid sheet into a conical shape that extends from the injector exit. Primary breakup occurs in a similar manner along both the upstream and downstream sides of the liquid jet (relative to the crossflow), which suggests relatively weak aerodynamic effects on the primary breakup. In the present study, the aerodynamic effects on the drop sizes in the wake region of the fuel injector were considered. The test conditions include different gas-to-liquid mass flow rate ratios and jet-to-freestream momentum flux ratios. The present measurements of the spray structure of aerated-liquid jets in crossflows shows a reduction in drop sizes with downstream distance that may be attributed to the drop secondary breakup.

Nomenclature

d	=	drop diameter
d_L	=	liquid sheet thickness
d_0	=	injector orifice diameter
GLR	=	aerating gas-to-liquid mass flow rate ratio
h	=	spray plume penetration height
h_0	=	nonaerated spray plume penetration height
M	=	Mach number
MMD	=	mass median diameter
Q	=	volumetric flow rate
Q_G	=	volumetric flow rate of gas injected
Q_L	=	volumetric flow rate of liquid injected
q_0	=	jet/freestream momentum flux ratio, $\rho_L^2 v_j^2/\rho_\infty u_\infty^2$
SMD	=	Sauter mean diameter for all droplets in the measuring volume, $\sum d_i^3/\sum d_i^2$
u	=	velocity component in the crossflow (horizontal) direction
u_∞	=	freestream velocity
v	=	velocity component in the jet streamwise (vertical) direction
v_j	=	jet exit velocity if all the injector exit area was occupied by the liquid phase, $W_L/(\pi d_o^2/4)$
w	=	width of the spray plume
x	=	cross-stream (horizontal) distance from the injector exit
y	=	streamwise (vertical) distance from the injector exit
z	=	spanwise (normal to the page) distance from the injector exit
β	=	flow-average void fraction
ρ	=	density

Subscripts

G	=	aerating gas property
j	=	jet exit property
L	=	liquid property
0	=	property at GLR = 0
∞	=	ambient gas property

Presented as Paper 1342 at the 45th AIAA Aerospace Sciences Meeting and Exhibit, Reno, NV, 8–11 January 2007; received 14 February 2007; revision received 11 July 2007; accepted for publication 13 July 2007.

*Graduate Student.
†Assistant Professor; khaled.sallam@okstate.edu. Member AIAA (Corresponding Author).
‡Assistant Professor.
§Senior Research Scientist. Associate Fellow AIAA.
¶Senior Aerospace Engineer. Member AIAA.

I. Introduction

AERATED injection is characterized by injecting a gas phase and a liquid phase together within the injector. At low gas-to-liquid mass flow rate ratios (GLR), the flow will exit the injector as a liquid jet with gas bubbles in the center of the jet. At higher GLR, however, the flow will exit as an annular flow consisting of a thin liquid film surrounding a gas core. The spray produced in the annular regime is made up of densely packed small droplets. This property of the spray makes it very useful for many applications, especially ramjet and scramjet applications [1], but it makes analyzing the spray difficult. Studies of spray structure have been performed downstream

in the less dense region using phase Doppler interferometry (PDI) by Lin et al. [2–4]. The properties at the injector exit were also measured by Sallam et al. [5]. They found that the underexpanded gas jet at the exit of the sonic (choked) injector passage forces the annular liquid sheet into a conical shape that extends from the injector exit. Primary breakup occurs along that liquid sheet in a similar manner along both the upstream and downstream sides of the liquid jet (relative to the crossflow), which suggests that there are relatively weak aerodynamic effects on the primary breakup. The secondary breakup in the near-injector region was not considered in this study. This leaves a gap of information about the aerodynamic effects on drop sizes between the less dense downstream area in the far field and the injector exit. This region is characterized by nonspherical droplets that are packed closely together. These nonspherical droplets prohibit the use of PDI in this area, and shadowgraphy is only able to capture a few droplets in focus, due to the limited depth of field associated with the high levels of magnification needed to measure the small droplets encountered in the spray. Holography techniques, however, ease the limitation on the depth of field and allow three-dimensional volumes of the spray at different locations to be measured. Therefore, a digital holographic technique was used In the present study, to penetrate this dense-spray region and measure these nonspherical droplets. The objectives of this study were to use a digital holographic technique to create three-dimensional maps of droplet sizes, which were used to observe the effects of different injection parameters on droplets sizes. The parameters studied were GLR, jet-to-freestream momentum ratio, and injector diameter. Changes in droplet sizes with downstream distance were measured to investigate whether secondary breakup might be occurring.

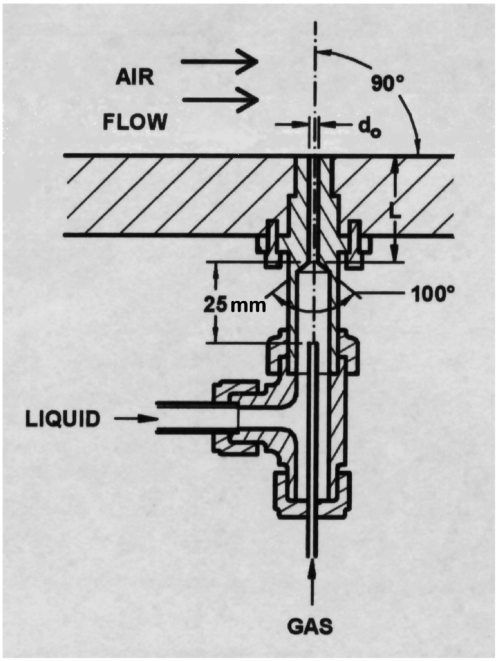

Fig. 1 Schematic of an aerated injector (inside out setup shown) (from [3]).

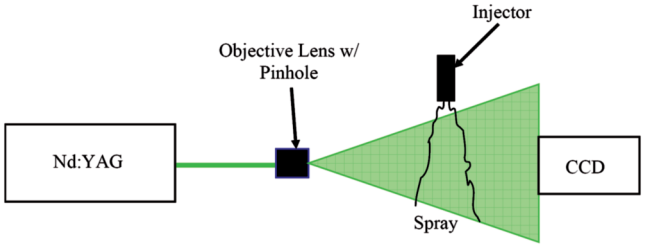

Fig. 2 Present optical setup.

II. Experimental Methods

A. Apparatus

Aerated-liquid injectors with exit diameters of 0.5 and 1.0 mm were used. These injectors consist of an inner tube for the aerating gas and an outer tube for the liquid, as shown in Fig. 1. The test liquid In the present study was tap water (referred to here as water) and the aerated gas was air. In ramjet and scramjet applications, however, fuels with lower surface tension (e.g., JP-8) are typically used, resulting in larger We number values and finer spray. The aerated-liquid jets were injected into a subsonic wind tunnel with a test section of $0.3 \times 0.3 \times 0.6$ m. The wind tunnel had float-glass side walls and floor and an acrylic ceiling to provide optical access. The air velocities in the test section were in the range of 3–60 m/s at

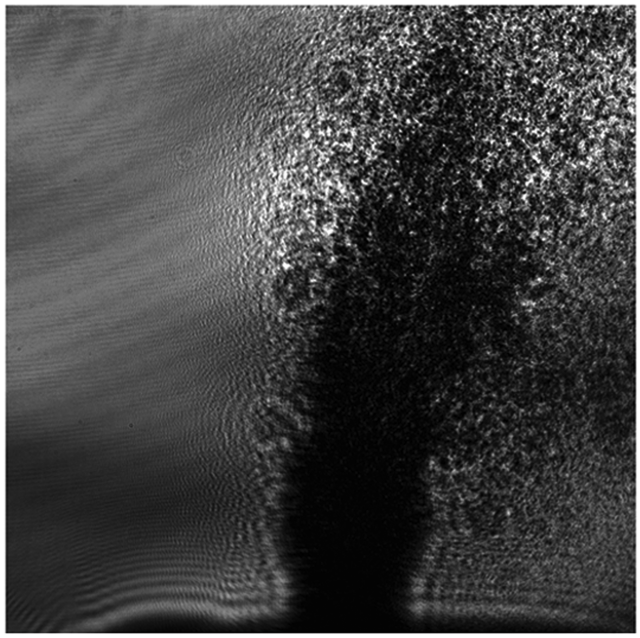

a)

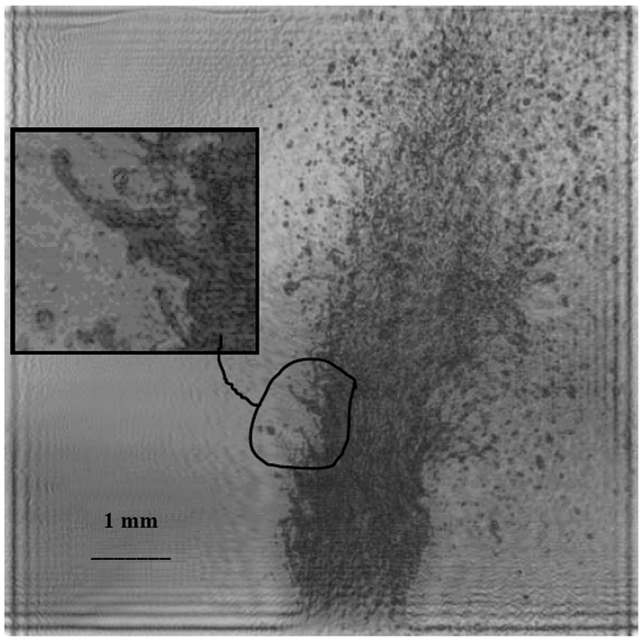

b)

Fig. 3 Hologram a) recorded at the injector exit with test conditions of GLR = 4%, $q_0 = 0.74$, and jet exit diameter $d_0 = 1$ mm (gaseous crossflow is from left to right) and b) reconstructed at the jet plane of symmetry; the inset shows an enlarged image of the circled ligament.

normal temperature and pressure. The air velocity in the test section was measured by a pitot-static tube (United Sensors model PDC-18-G-16-KL) installed at the end of the test section. The pitot-static tube was connected to an inclined tube manometer (Dwyer model 400-10-Kit). Air velocities in the wind tunnel could be measured within $\pm 2\%$. The wind tunnel had a contraction ratio greater than 16:1, and the velocity variation inside the test section was less than $\pm 1\%$ of the mean freestream velocity. The air boundary-layer thickness was estimated to be less than 0.5 mm at the injection location. The test liquid was contained within a cylindrical liquid supply chamber having a diameter of 100 mm and a length of 300 mm, constructed of type 304 stainless steel. The liquid was forced through the injector by admitting high-pressure air to the top of the chamber. The aerating gas travels through the inner tube and passes through several 100-μm holes located near the end of the tube. At sufficient GLRs (greater than 2%), the gas and liquid mix to form a two-phase flow, which consists of a gas core surrounded by a thin liquid sheet (annular regime). The air and liquid flow rates were then controlled by rotameter-type flow meters (the air flow meter was OMEGA model 044-40NCA and the water flow meter was OMEGA model N034-39G). The air flow meter could read flow rates ± 3 cm^3/s, and the water flow meter could read flow rates ± 0.02 cm^3/s. The uncertainty in the flow rate measurement is 6%. The high-pressure air was kept in a storage tank with a volume of 0.18 m^3 and provided an injection pressure of 1.1 MPa.

B. Instrumentation

Two methods of digital holography were considered: in-line digital holography and digital holographic microscopy. In previous work in this lab [6], in-line digital holography was chosen to study the spray of aerated injectors because of its ability to capture a large field of view and its experimental setup simplicity. This technique, however, would not provide the resolution required to resolve the smallest droplets in the spray. For higher magnification but smaller field of view, digital holographic microscopy [7] was used in the present study. This technique removes some of the lenses that were necessary in the in-line setup, which greatly reduces the number of aberrations introduced by lenses. The optical setup shown in Fig. 2 consists of only one laser beam, which was expanded with a 5× objective lens and then passed directly through the test section to a cooled interline transfer CCD camera (Cooke model PCO 2000) having 2048×2048 pixels that were 7.4 μm wide by 7.4 μm tall.

After the hologram was recorded, as shown in Fig. 3a, it was reconstructed, as shown in Fig. 3b, using the convolution-type approach that solves the Rayleigh–Sommerfeld formula for reconstruction of a wave field by the use of the fast Fourier transform algorithm [8]. The method of average-intensity subtraction is used in the current hologram reconstruction, and the current setup neglects the out-of-focus virtual image, because its effect is small enough that droplets can still be resolved and measured accurately. Using this method, the smallest measurable droplets with diameters of 17 μm were measured with uncertainties of 50%. The Sauter mean diameter (SMD) was calculated by measuring a large number of droplets within the measuring volume captured on multiple holograms. Samples consisting of 30–300 droplets were used at each data point to determine the SMD. The SMD uncertainty was less than 30% (within a 95% confidence level), dominated by the sampling limitations when few drops appeared near the edge of the spray and in the central region of the spray. The smallest SMD size in the present study was 59 μm. Droplets of this size could be measured with an uncertainty of 15%. Irregular drops were assumed to be ellipsoids and were assigned diameters equal to the diameter of the sphere having the same volume as the ellipsoid. Reconstructions were made with 1-mm increments, and hence the location of the centroid of the droplet can be known within ± 1 mm. Measurements in the x and y directions were determined by the placement of the camera when the holograms were recorded. The placement of the camera could be determined ± 2 mm.

III. Results and Discussion

Single-pulsed holograms were captured for different test conditions, as shown in Tables 1 and 2. Each hologram was then reconstructed numerically. A typical reconstructed hologram is shown in Fig. 4 for the following test conditions: GLR = 4%, $q_0 = 0.74$, $d_0 = 1$ mm, $x/d_0 = 25$, and $y/d_0 = 30$. Figure 4 shows the reconstruction of the hologram at the $z/d_0 = 6$ plane with a field of view of 9×9 mm captured on 2048×2048 pix. The measurements of droplet sizes and locations were presented as three-dimensional maps of the SMD for different test conditions. The

Table 1 Summary of results for the 0.5-mm injector

D_0, mm	0.5	0.5	0.5	0.5	0.5	0.5	0.5	0.5
M	0.16	0.16	0.16	0.16	0.07	0.07	0.07	0.07
x/d_0	25	50	25	50	25	50	25	50
Q_0	0.74	0.74	0.74	0.74	4	4	4	4
GLR %	4	4	8	8	4	4	8	8
Q_L, cm^3/s	0.33	0.33	0.33	0.33	0.33	0.33	0.33	0.33
Q_G, cm^3/s	10.8	10.8	21.7	21.7	10.8	10.8	21.7	21.7
SMD, μm	154	97	75	62	168	149	74	70
h/d_0 Lin et al. [4]	38	50	45	59	89	117	109	143
h/d_0present	60	90	60	90	120	180	120	180
$w/2d_0$ Lin et al. [4]	12.7	17.3	12.7	17.3	15	20.5	15	20.5
$w/2d_0$present	22	22	17	22	22	30	24	28

Table 2 Summary of results for 1.0-mm injector

d_0, mm	1.0	1.0	1.0	1.0	1.0	1.0	1.0	1.0
M	0.18	0.18	0.18	0.18	0.075	0.075	0.075	0.075
x/d_0	25	50	25	50	25	50	25	50
q_0	0.74	0.74	0.74	0.74	4	4	4	4
GLR %	4	4	8	8	4	4	8	8
Q_L, cm^3/s	1.45	1.45	1.45	1.45	1.45	1.45	1.45	1.45
Q_G, cm^3/s	49	49	103	103	49	49	103	103
SMD, μm	151	118	72	59	164	106	86	73
h/d_0 Lin et al. [4]	27	35	33	43	68	90	87	115
h/d_0present	45	60	60	75	105	120	90	120
$w/2d_0$ Lin et al. [4]	12.7	17.3	12.7	17.3	15	20.5	15	20.5
$w/2d_0$present	12.5	18.5	14.5	21	19.5	25	21.5	25.5

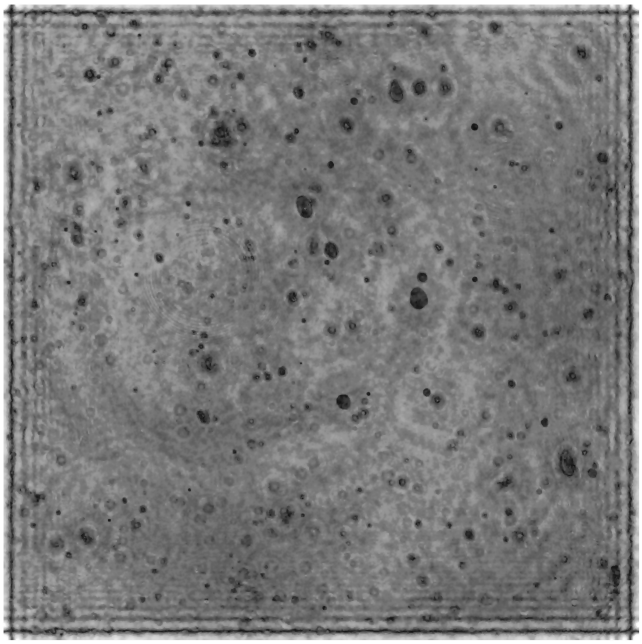

Fig. 4 Reconstruction of digitally recorded hologram at $x/d_0 = 25$, $y/d_0 = 30$, and $z/d_0 = 6$. The test conditions were GLR = 4%, $q_0 = 0.74$, and $d_0 = 1$ mm. The field of view of this figure is 9 × 9 mm.

orientation of these maps is similar to Fig. 5. The results of SMD are summarized in Table 3.

A. Effect of the GLR

Changing the GLR had the most effect over the droplet sizes. Figure 6 shows this effect. The SMD for the entire population at the condition of $d_0 = 1$ mm and $q_0 = 0.74$ is reduced from 151 to 71 μm when the GLR is increased from 4 to 8%. This is due to the liquid film being "squeezed" into a thinner sheet, due to the increased gas flow rate. The equation that describes this liquid film thickness is given by Lin et al. [2] as follows:

$$d_L = d_0(1 - \beta^{1/2})/2 \tag{1}$$

where d_0 is the nozzle exit diameter and β is the flow-average void fraction given by Lin et al. [2] as

$$\beta = Q_G/(Q_G + Q_L) \tag{2}$$

In this equation, the variables Q_G and Q_L are the volumetric flow rates of the gas and liquid, respectively. If the SMD is normalized by this film thickness, which is controlled by the GLR, the values will be on the same order of magnitude. This shows that the droplet size is not controlled by the jet diameter, but by the GLR, which controls the film thickness.

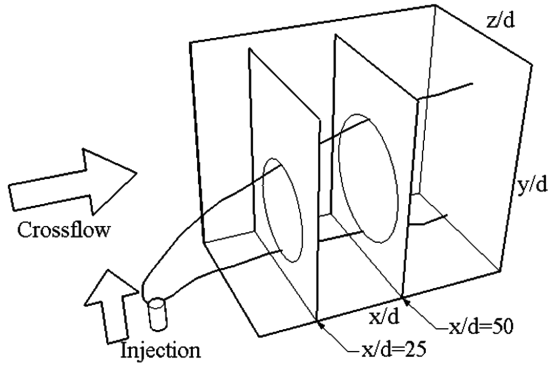

Fig. 5 Sketch showing the orientation of the SMD plots.

The penetration height of the spray plume is also affected by different GLRs. When comparing the two different GLRs in Fig. 6, the 8% GLR condition results in a height difference of 15 jet diameters. This is due to the thinner liquid sheet exiting the injector at a higher velocity than the thicker liquid sheet at the lower GLR. A correlation for this height has been reported by Lin et al. [4]:

$$(h - h_0)/d_0 = 0.9(\mathrm{GLR})^{0.46} M^{-0.64} q_0^{0.34} (x/d_0)^{0.39} \tag{3}$$

where

$$h_0/d_0 = 3.17 q_0^{0.33} (x/d_0)^{0.40} \tag{4}$$

where h is the penetration height, h_0 is the nonaerated penetration height, q_0 is the jet-to-freestream momentum ratio, and M is the freestream Mach number. The predicted penetration heights given by this correlation are listed in Tables 1 and 2 with the measured values in the present study. The difference between the two may be attributed to the fact that in Lin et al. [4], the penetration heights in the far field ($x/d_0 > 100$) are determined using a threshold of 0.01 $\mathrm{cm^3/s/cm^2}$, whereas in the present measurements, the location of the highest drop in the spray at that downstream location was taken as the penetration height. The present measurements of h/d_0 listed in Tables 1 and 2 are therefore labeled as the maximum h/d_0.

Lin et al. [4] stated that the GLR has little effect on the width of the spray plume. This also holds true in the current results. The correlation given for the width of the spray plume w is given [4] as

$$w/2d_0 = 3.07 q_0^{0.10} (x/d_0)^{0.45} \tag{5}$$

These predicted values are listed in Tables 1 and 2, along with the present measurements. The present measurements are the maximum width of the spray, and so they are expected to be larger than the

Table 3 Drop-size reduction between $x/d_0 = 25$ and 50 for each of the test conditions

d_0, mm	GLR	q_0	v_∞, m/s	v_{jet}, m/s	x/d_0	SMD, μm	Reduction in SMD
1	4%	0.74	61	64	25	151	
1	4%	0.74	61	64	50	118	22%
1	4%	4	26	64	25	164	
1	4%	4	26	64	50	106	35%
0.5	4%	0.74	56	56	25	154	
0.5	4%	0.74	56	56	50	97	37%
0.5	4%	4	24.2	56	25	168	
0.5	4%	4	24.2	56	50	149	11%
1	8%	0.74	61	133	25	72	
1	8%	0.74	61	133	50	59	18%
1	8%	4	26	133	25	86	
1	8%	4	26	133	50	73	15%
0.5	8%	0.74	56	112	25	75	
0.5	8%	0.74	56	112	50	62	17%
0.5	8%	4	24.2	112	25	74	
0.5	8%	4	24.2	112	50	70	5%

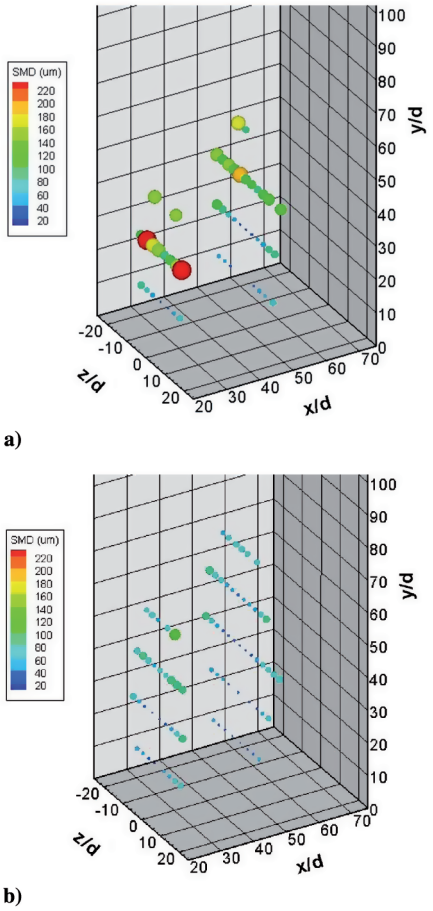

Fig. 6 Effect of GLR: a) SMD distribution at GLR = 4%, , $q_0 = 0.74$, and $d_0 = 1$ mm and b) SMD distribution at GLR = 8%, $q_0 = 0.74$, and $d_0 = 1$ mm.

predicted value that defines the edge of the spray as the place at which the volume flux is greater than 0.01 $cm^3/s/cm^2$.

B. Effect of the Jet Exit Diameter

When the spray produced by the 1-mm injector is compared with the 0.5-mm injector, the effects on the drop size are small, similar to earlier observations in the far field ($x/d_0 > 100$) by Lin et al. [4]. These effects can be seen in Table 3. The SMD distribution of the sprays remained relatively constant when only the jet exit diameter was changed. This is most likely due to the fact that the droplet size is controlled more by the thickness of the liquid sheet exiting the injector, which is controlled by the GLR, than to the physical size of the jet diameter. The most significant effect the jet diameter had on the spray was on the number of droplets that were observed for the same test conditions. Although the SMD distribution of the spray remained relatively constant, the number of the droplets observed in the case of the large injector was nearly double the number of droplets for the small injector. This is due to the fact that the flow rate of the liquid that was injected using the smaller injector ($Q_L = 0.33$ cm^3/s) was lower than the flow rate of the liquid being injected into the larger injector ($Q_L = 1.45$ cm^3/s). This was done so that the q_0 would remain constant for different jet diameters.

C. Effect of the Jet/Freestream Momentum Flux Ratio

The main effect of the jet/freestream momentum flux ratio was controlling the spray plume penetration, which agrees with the findings of Lin et al. [1–4]. The two jet/freestream momentum flux ratios investigated were $q_0 = 0.74$ and 4. This effect can be seen in Fig. 7. As expected, the $q_0 = 4$ condition provided larger penetration heights than the $q_0 = 0.74$ condition. The jet/freestream momentum flux ratio also has an effect on the spray plume width. As predicted by

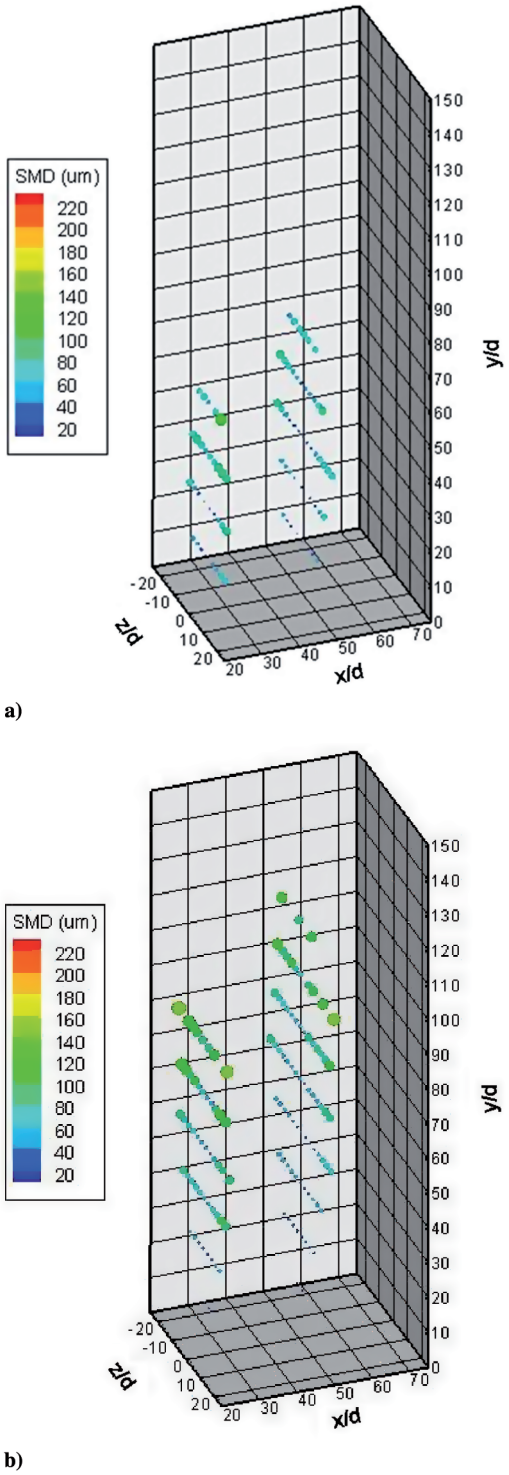

Fig. 7 Effect of q_0: a) SMD distribution at GLR = 8%, $q_0 = 0.74$, and $d_0 = 1$ mm and b) SMD distribution at GLR = 8%, $q_0 = 4$, and $d_0 = 1$ mm.

Eq. (5), as q_0 increases, so does the spray plume width. It can be seen from Tables 1 and 2 that at the higher values of q_0, the spray plume is wider than at similar conditions with a lower value of q_0.

D. Effect of the Downstream Location

Major changes in droplet sizes as they travel downstream may imply that secondary breakup occurred between the two locations. It is expected that the droplet diameters should shrink some amount as they travel downstream due to evaporation, but large changes may indicate that something else is taking place: namely, secondary

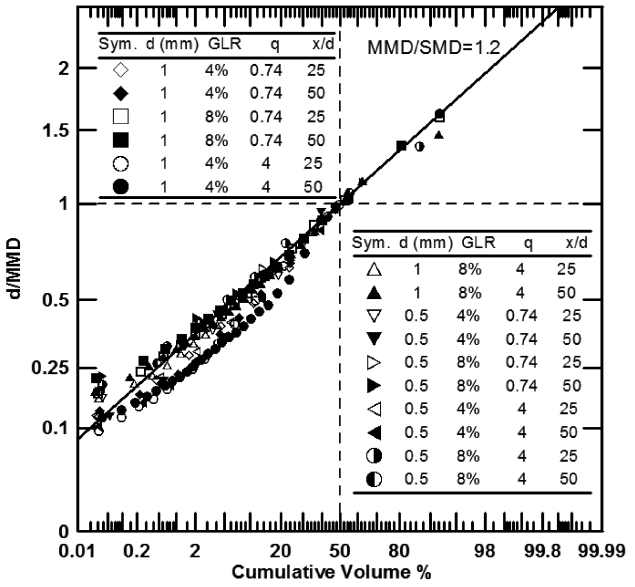

Fig. 8 Droplet size distribution plot.

breakup. The measured values of overall SMD are listed in Table 3. At the 8% GLR conditions, there is little or no change between the two downstream distances, but at all of the 4% GLR conditions, there is a considerable reduction in SMD of up to 60 μm. This could be evidence of secondary breakup in this region. To determine if secondary breakup is occurring, the droplets' velocities should be measured and the droplets' Weber numbers should be calculated in the questionable region. According to Hsiang and Faeth [9] drops will begin breaking up at a Weber number of around 10. Other properties such as spray plume penetration and spray plume width are also affected by downstream distance. It is evident that the spray is continuing to increase in height and width as it travels from $x/d_0 = 25$ to 50. This means that the droplets are still retaining their initial momentum and did not relax to the local conditions.

E. Overall Droplet Distribution

Simmons [10] showed that a universal linear correlation for drop-size/volume-fraction distributions of sprays can be established for all fuel nozzles if the drop sizes are normalized by their mass median diameter (MMD) and plotted on a root-normal scale. Using this correlation, the volume fractions corresponding to any drop-size range can be estimated given the MMD or the SMD. Figure 8 shows the present data plotted according to Simmons. It can be seen that the majority of these data points at GLR = 8% follow Simmons's universal root-normal distribution with MMD/SMD = 1.2. However, for some of the test conditions of 4% GLR, the values fall below this line. This could be due the presence of few large drops in the spray, which sets the MMD at a higher value and consequently shifts the whole distribution down.

IV. Conclusions

The present work probed the spray of aerated injectors in subsonic crossflow in the optically challenging near-injector area. The major conclusions are as follows:

1) Digital holography is a useful tool for examining this dense near-injector area and can provide information that other methods cannot. This is due to the fact that it is insensitive to the droplets being nonspherical in this region.

2) Digital holographic microscopy works better than the standard digital in-line holography [6]. It removes a substantial amount of noise because of the elimination of the additional lenses needed with the in-line method.

3) As the GLR increased from 4 to 8%, droplet sizes decreased. The droplet sizes were independent of other variables such as injector diameter. Jet-to-freestream momentum flux ratio had little effect on droplet size. Drop sizes were found to correlate with the film thickness, which is a function of the GLR.

4) Reductions in droplet sizes at the GLR = 4% conditions between the two downstream locations of $x/d_0 = 25$ and 50 showed signs of secondary breakup. Further investigation of the droplets' Weber numbers is needed to confirm this conclusion.

Acknowledgments

Support from Taitech, Inc., under a subcontract with the U.S. Air Force Research Laboratory and from a NASA Oklahoma Space Grant Consortium Fellowship for the first author (B. Miller) is gratefully acknowledged. Initial development of experimental methods was carried out under the National Science Foundation grant EPS-0132534 (Oklahoma-EPSCOR). The U.S. Government is authorized to make copies of this article for governmental purposes notwithstanding any copyright notation thereon.

References

[1] Lin, K.-C., Kennedy, P. J., and Jackson, T. A., "Penetration Heights of Liquid Jets in High-Speed Crossflows," 40th AIAA Aerospace Sciences Meeting and Exhibit, AIAA Paper 2002-873, 2002.

[2] Lin, K.-C., Kirkendall, K. A., Kennedy, P. J., and Jackson, T. A., "Spray Structures of Aerated Liquid Fuel Jets in Supersonic Crossflows," 35th AIAA/ASME/SAE/ASEE Joint Propulsion Conference and Exhibit, AIAA Paper 1999-2374, 1999.

[3] Lin, K.-C., Kennedy, P. J., and Jackson, T. A., "Spray Structures of Aerated-Liquid Jets in Subsonic Crossflows," 32nd AIAA Aerospace Sciences Meeting, AIAA Paper 2001-0330, 2001.

[4] Lin, K.-C., Kennedy, P. J., and Jackson, T. A., "Structures of Aerated Liquid Jets in High Speed Crossflows," 32nd AIAA Fluid Dynamics Conference, AIAA Paper 2002-3178, 2002.

[5] Sallam, K. A., Aalburg, C., Faeth, G. M., Lin, K.-C., Carter, C. D., and Jackson, T. A., "Primary Breakup of Round Aerated-Liquid Jets in Supersonic Crossflows," *Atomization and Sprays*, Vol. 16, No. 6, 2006, pp. 657–672. doi:10.1615/AtomizSpr.v16.i6.40

[6] Miller, B., Sallam, K. A., Lin, K.-C., and Carter, C., "Digital Holographic Spray Analyzer," Fluids Engineering Div., American Society of Mechanical Engineers, Paper FEDSM2006-98526, 2006.

[7] Schnars, U., and Jueptner, W., *Digital Holography: Digital Hologram Recording, Numerical Reconstruction, and Related Techniques*, Springer, Berlin, 2005.

[8] Kreis, T. M., Adams, M., and Jüptner, W. P. O., "Methods of Digital Holography: A Comparison," *Proceedings of SPIE: The International Society for Optical Engineering*, Vol. 3098, Sept. 1997, 224–233. doi:10.1117/12.281164

[9] Hsiang, L.-P., and Faeth, G. M., "Drop Deformation and Breakup Due to Shock Wave and Steady Disturbances," *International Journal of Multiphase Flow*, Vol. 21, No. 4, 1995, pp. 545–560. doi:10.1016/0301-9322(94)00095-2

[10] Simmons, H. C., "The Correlation of Drop-Size Distributions in Fuel Nozzle Sprays, Part 1: The Drop-Size/Volume-Fraction Distribution," *Journal of Engineering for Power*, Vol. 99, No. 3, 1977, pp. 309–319.

D. Talley
Associate Editor